ただし，ガイドワイヤの根元の部分はカテーテル内に挿入されているとし，その部分では血管ではなく，カテーテルとの間で接触判定をした．

2.4　解析手順

2.1～2.3で述べた条件をもとに，式(1)の運動方程式を可変次数の数値微分公式（NDF）を用いて解析した．すなわち，微少時間ステップごとに個々のセグメントの接触力とそれに起因するモーメントのそれぞれの和を求め，逐次的に解くことでリンクの挙動を計算した．ただし，時間ステップは可変であり，各時間ステップにおける相対誤差が許容値（10^{-4}）以内になるように細かくした．また，各時間ステップ間でモデル間に接触が起きた場合は，その間で内挿ステップをとった．

3．簡単な血管モデルを用いた計算例

本シミュレータのように，カテーテルの経路を定量的に算出するためには，シミュレーションに用いるパラメータを適切に設定することが不可欠である．一方，ガイドワイヤの操作のためには，体外からガイドワイヤに押し・引きおよびねじりの動作を加えることにより操作をする．そのため，簡単なトーラス形状の血管モデルの中でガイドワイヤモデルに押し，ねじり動作を個別に加え，シミュレーションに用いる血管およびガイドワイヤの基本的なパラメータの検討を行った（Fig. 1）．すなわち，それぞれのパラメータを基本条件から個別に変化させ，ガイドワイヤ先端の挿入軌道・接触力などに与える影響を調べた．ガイドワイヤの物性および形状の基本条件となるパラメータについては，市販されているガイドワイヤの物性および形状を測定したものをもとに設定した．血管反力の弾性係数（K_i）としては，2軸に引っ張った血管切片を用いた摩擦実験[15]をもとに設定した．また，ここでは先端40mmのみを計算に用いたが，途中の部分についての結果はオフセットとして加えればよいと考えられる．

3.1　押し／引き方向

まず，ねじりの動作は考慮せず，ガイドワイヤモデルの根元を一定速度（5 mm/s）で挿入した．結果を以下にまとめる(詳細については参考文献[11]を参照されたい)．

- ガイドワイヤと血管の間の摩擦係数を大きくすると，ガイドワイヤ先端の位置および接触力が大きく振動した．先端の軌道は振動するものの最終的な軌道はあまり変わらなかった．
- 球と平面のヘルツ接触理論の式[16]より脳底動脈の増分弾性係数[17]をヤング率として血管の反発力を計算するとガイドワイヤが血管の初期位置から大きくはみ出てしまった．そのため，血管が周囲組織によって係留される力も反力に含める必要があると考えられる．
- ガイドワイヤ先端に屈曲をつけることにより，血管の屈曲部での反発力が軽減された．
- ガイドワイヤの曲げ剛性を大きくすると，血管の変形が大きくなった．

3.2　ねじり方向

前節ではガイドワイヤをねじる動作は行なわなかったが，ねじりは実際の手技の中で多用される．例えば，あらかじめ先端を屈曲させておいて，分岐部でねじりを加えてさらに押しこむことによって，分岐部の選択を行なう．また，実際の手術では，先端に適切な屈曲をつけたガイドワイヤをねじって血管壁との接触角度が最小になるようにして，接触力の低下を図っている．実際，前節ではガイドワイヤ先端に屈曲をつけることによって血管との接触力が低下することを示した．そのため，本節では，先端に屈曲のついたガイドワイヤを30 mm挿入させ，その位置から根元に一定速度（45 degree/s）でねじり動作を加えて，モデルのねじり方向のパラメータのトルク伝達性への影響を評価した．ガイドワイヤのトルク伝達性としては，ガイドワイヤの根元に加えられた動きが時間遅れなく，なめらかに先端まで伝わることが求められる．主な結果を以下にまとめる（詳細については参考文献[12]を参照されたい）

- 先端まで力の伝達が始まるまでに時間遅れが確認できた．また，ガイドワイヤと血管の間の摩擦係数を大きくすると，先端の追従性が悪くなり，大きく振動している場合もあった．
- 血管の屈曲を増やしても，屈曲の位置によっては，ガイドワイヤの先端の追従性がよくなった（Fig. 2）．

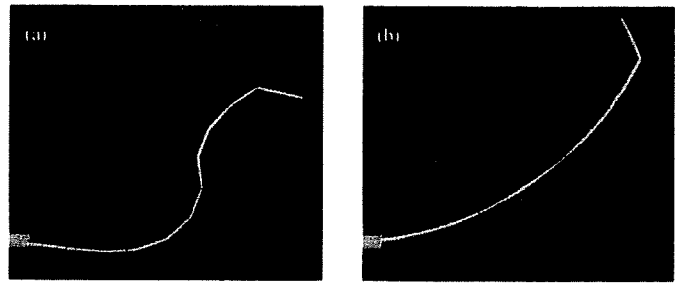

Fig. 2 Simulation model (a) immediately after rotation (b) after rotation for 4 seconds.

・ガイドワイヤの剛性を大きくすると，血管の追従性がよくなった．

3.3 ガイドワイヤの選定

ガイドワイヤを手術に用いる場合，血管内での押し／引き方向の推進力の伝達性とねじり方向の先端の追従性が求められる[18-22]．その観点から考えると，3.1は推進力の伝達性の評価，3.2は追従性の評価に相当する．

トルク伝達特性を評価基準としてガイドワイヤを評価した場合，3.2で得られた結果から，摩擦係数の小さく剛性の大きいガイドワイヤを選択することが望ましい．市販されているガイドワイヤは，Fig. 3のような構造になっているものが多い．このような構造の場合，表面のコーティングを変えることにより摩擦係数を減らすことを，金属線の太さやヤング率を大きくすることによって剛性を，個別に良化することが可能である．

しかし，ガイドワイヤの評価基準としては，トルク伝達性以外にもさまざまある．例えば，3.1のように挿入する際に血管に加えられる力で評価すると，剛性が大きくなると，接触力も大きくなり望ましくない．一方，先端の柔軟性は，血管の屈曲に沿って挿入していくために必要であるが，やわらかすぎると，途中で座屈してしまう恐れもある．さらには，本研究で行なったようにカテーテルを固定させてガイドワイヤを挿入したあと，実際は固定させたガイドワイヤに沿ってカテーテルを挿入させる．このとき，ガイドワイヤの剛性が弱すぎると，ガイドワイヤが動く恐れがある[23]．

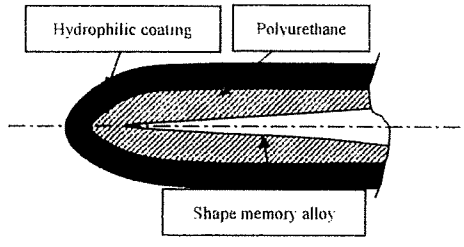

Fig. 3 Structure of flexible guidewire tip.

そのため，剛性と柔軟性のトレードオフに対して，パラメータのバランスを考えて設計することが必要である．しかし，式(7)のように曲げ・ねじりのパラメータを独立に決めることは難しく，その効果も不明な点が多い．さらに3.2で示したように血管の形状によっては，同じガイドワイヤでもトルク伝達性は変化する．そのため，シミュレータを用いて設計を行い，さらに症例ごとに術前に計算してガイドワイヤを使い分ければ，その効果も大きくなる．例えば，ガイドワイヤの剛性が小さくてもトルク伝達性が得られるような血管形状であれば，血管の損傷を与えないように柔軟なガイドワイヤを使うことが考えられる．

4．医用画像を用いた計算例

前節のように得られたパラメータを用い，病変部を撮影した医用画像より作成した血管モデルを用いた計算例をFig. 4に示す．Fig. 4はもともと動画であり，患者個別に治療方法を説明するためのコミュニケーションツールとして使用できる．特に，脳動脈瘤の血管内外科治療をするためには，症状のない未破裂の状態で治療を行なう場合が多く，手術に伴うリスクについて患者に的確に説明する必要があろう．

医用画像を用いたシミュレーションでは，複雑

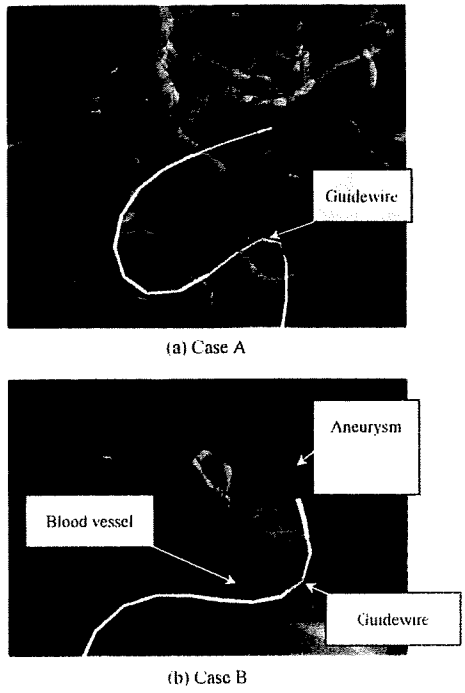

Fig. 4　An example of visualization after catheter simulation with this system

な3次元血管形状を定量的に表現し，その特徴量をもとに解析結果を解釈する必要がある．一方，脳動脈瘤の発生および破裂には，例えば，嚢状動脈瘤がWillis動脈輪分岐部に好発するように特徴的な血管形状，およびそれに起因する血行動態が深く関与していると推測されている[24]．このように動脈瘤の発生は血管形状の影響を受けるので，血管内治療の対象となる血管形状としても何らかの特徴が見出せるかもしれない．今後，本シミュレータでの計算結果をデータベース化し，統計処理により脳血管形状との関係性を検討していく予定である．当然，支配する物理法則が違うので，単純には結び付けられないとは思うが，血管内治療の難しさについても血管の形状をもとにした指標で評価できるようになるかもしれない．

5．おわりに

本稿では著者らが開発している脳血管内でカテーテルを安全に操作誘導するための術前・術中におけるカテーテル経路予測用シミュレータについて解説した．さらに簡単な血管モデルを用いた基本的なパラメータの検討結果について示した．今後，CTやMRIなどの医用画像から患者個別の症例に対応した血管モデルの構築を行ない，モデルの精度向上および実際の血管形状や部位による影響を検討していく予定である．

謝　辞

本研究にあたり，福山通運渋谷長寿健康財団松下珠美様にご助力を頂いた．ここに謝意を表する．

文　献

1) Martin, R.W and Johnson, C.C.: Design characteristics for intravascular ultrasonic catheters. International Journal of Cardiac Imaging, 4 (2-4). 201-216, 1989.
2) Wang, Y Chui, C., Lim, H. Cai, Y and Mak, K. Real-time interactive simulator for percutaneous coronary revascularization procedures. Computer Aided Surgery. 3 (5) 211-227 1998.
3) Lawton, W. Raghavan, R. Ranjan, S.R. and Viswanathan, R.R.: Tubes in tubes: catheter navigation in blood vessels and its applications. International Journal of Solids and Structures, 37 (22). 3031-3054, 2000.
4) Dawson, S.L Cotin, S. Meglan, D. Shaffer D.W. and Ferrell, M.A. Designing a computer-based simulator for interventional cardiology training. Catheterization and Cardiovascular Interventions, 51 (4). 522-527 2000.
5) 山村直人，姫野龍太郎，牧野内昭武：カテーテルシミュレータの開発―ガイドワイヤーのシミュレーションに関する検討―，理研シンポジウム“生体力学シミュレーション研究”予稿集，136-144, 2003.
6) Konings, M.K. van de Kraats, E.B. Alderliesten, T. and Niessen, W.J Analytical guide wire motion algorithm for simulation of endovascular interventions. Medical & Biological Engineering &

Computing, 41 (6), 689-700, 2003.
7) Bruijns, J., Peters, F.J., Berretty, R.P.M., van Overveld, C.W.A.M. and ter Haar Romeny, B.M. Fully automatic computation of the shape of a micro-catheter International Congress Series 1281, 401-406, 2005.
8) Bhat, S., Kesavadas, T and Hoffmann, K.R. A physically-based model for guidewire simulation on patient-specific data. International Congress Series 1281, 479-484, 2005.
9) Cai, Y.Y Chui, C.K. Ye, X.Z. Fan, Z and Anderson, J.H. Tactile VR for hand-eye coordination in simulated PTCA. Computers in Biology and Medicine, 36 (2) 167-180, 2006.
10) Schafer S., Singh, V Hoffmann, K.R., Noel, P.B., and Xu, J.: Planning image-guided endovascular interventions: guidewire simulation using shortest path algorithms, Proceedings of SPIE, 6509, 65092C, 2007
11) 高嶋一登，大田慎二，太田信，葭仲潔，池内健：カテーテルシミュレータの開発（第1報，ガイドワイヤ・血管の特性の評価），日本機械学会論文集，C-072 (719)，2137-2144，2006.
12) 高嶋一登，大田慎二，太田信，葭仲潔，向井利春：カテーテルシミュレータの開発（第2報，ガイドワイヤのトルク伝達性の評価），日本機械学会論文集，C-73 (735)，116-123，2007.
13) 吉川暢宏，李 源培：一次元柔軟構造物のファーストオーダー設計モデル，計算工学講演会論文集，6 (2)，785-788，2001.
14) 吉田和司，河内政隆：軟質媒体の変形挙動解析（第1報,紙葉類のばね—質量梁モデルの検討），日本機械学会論文集，A-58 (552)，1474-1480，1992.
15) Takashima, K. Shimomura, R. Kitou, T Terada, H. Yoshinaka, K. and Ikeuchi, K. Contact and friction between catheter and blood vessel. Tribology International, 40 (2), 319-328, 2007
16) Timoshenko, S.P and Goodier J.N. Theory of Elasticity 3rd ed. McGraw-Hill, 1970.
17) Hayashi, K., Nagasawa, S., Naruo, Y. Okumura, A. Moritake, K. and Handa, H. Mechanical properties of human cerebral arteries, Biorheology, 17 (3), 211-218, 1980.
18) Schroder J. The mechanical properties of guidewires. Part I: Stiffness and torsional strength. Cardiovascular and Interventional Radiology, 16 (1) 43-46, 1993.
19) 座古勝，高野直樹，倉敷哲生，奥出修平，西部淳：医療用カテーテルの力学的特性評価手法に関する研究，日本材料学会学術講演会講演論文集，49，213-214，2000.
20) Sutou, Y Yamauchi, K. Suzuki, M. Furukawa, A. Omori, I Takagi, I Kainuma, R. Nishida, M. and Ishida, K. High maneuverability guidewire with functionally graded properties using new superelastic alloys. Minimally Invasive Therapy and Allied Technologies, 15 (4) 204-208, 2006.
21) Ceschinski, H., Henkes, H., Weinert, H. C., Weber W Kuhne, D. and Monstadt, H. Torquability of microcatheter guidewires: the resulting torsional moment. Bio-Medical Materials and Engineering, 10 (1) 31-42, 2000.
22) Schmitz, K. P Behrens, P Schmidt W Behrend, D. and Urbaszek, W Quality determining parameters of balloon angioplasty catheters. J Invasive Cardiol, 8 (3) 144-152, 1996.
23) Schroder J. The mechanical properties of guidewires. Part III: Sliding friction. Cardiovascular and Interventional Radiology, 16 (2) 93-97 1993.
24) 氏家弘：脳動脈瘤と血流，日本バイオレオロジー学会誌，15 (1)，29-32，2001.

第30回日本バイオレオロジー学会年会
（2007年6月14～15日 札幌）にて発表

Studies on Design Optimization of Coronary Stents

K. Srinivas[1]
e-mail: k.srinivas.usyd.edu.au

T. Nakayama

M. Ohta

S. Obayashi

Institute of Fluid Science,
Tohoku University,
2-1-1 Katahira, Aoba-ku,
Sendai 980-8577, Japan

T. Yamaguchi
Department of Bioengineering and Robotics,
Graduate School of Engineering,
Tohoku University,
Aoba 1,
Sendai 980-8579, Japan

The stent design itself seems to be one of the factors responsible for restenosis. As a remedy, the present work attempts to perform a design optimization of coronary stents from a hemodynamic point of view. For the purpose, we have applied the principles of modern exploration of design space restricting ourselves to two-dimensional considerations. Width, thickness, and spacing of the struts of the stent formed the design variables. The objectives chosen for optimization were the vorticity generated, length of recirculation zone, and the reattachment distance in between the struts. Both semicircular and rectangular cross sections of stents were included. Starting with the range of design variables, sample stent cases were generated using Latin hypercube sampling. Objective functions were calculated for each of these by computing the two-dimensional flow using software FLUENT under the assumption of a steady, Newtonian flow considering a model stent with three struts. This was followed by Kriging to construct a response surface, which gives the relationship between the objectives and the design variables. The procedure gave nondominated fronts, which consist of optimized designs. Stents with minimum vorticity, with minimum recirculation distance, and the ones with maximum reattachment length in between struts were generated. The procedure is capable of producing the optimum set of design variables to achieve the prescribed objectives.
[DOI: 10.1115/1.2885145]

Keywords: stent, coronary stent, stenosis, restenosis, optimization

1 Introduction

A stent is placed in the blood vessel to remedy stenosis, a condition where in the vessel is blocked reducing the effective area for flow. The stent widens the passage to restore the flow. However, literature reveals that restenosis may take place in as many as 25–50% of the cases, see, for example, Grewe et al. [1], while using bare metal stents. Studies have shown that the drug eluting stents give a much smaller rate of restenosis, typically 3–9% [2]. Previous work [3–5] suggests that after the vessel size, the stent design is the most important factor in determining the rate of restenosis.

There have been many experimental and computational studies of flow through a stented blood vessel [5–10]. Computations use mostly the methods in computational fluid dynamics where progress has been made to such an extent that it has been possible to compute patient specific cases [11,12]. There have also been studies on structural aspects of stents; a good account of these is given by Whittaker and Fillinger [13] and Lally et al. [3]. Following the developments in related fields such as aerospace and automobile engineering, a natural extension of the work seems to be one of optimization, which itself has become a significant discipline in industry today. We have started an ambitious program to carry out a design optimization of stents. This paper describes some of our preliminary results.

Optimization relies on what are called fitness or objective functions, which may have to be minimized or maximized depending on their nature. What features of flow one selects for these functions depend on what one desires in an ideal stent. A great deal of information has been collected on the stent behavior and the flow through a stented vessel in the previous studies. A review of these helps in formulating the objective functions.

It appears that wall shear stress (WSS) and recirculation of flow are the crucial features that influence restenosis. A low WSS is found to make way for the intimal thickening [14] in the vessel, which becomes pronounced when the gap between struts is a minimum. It is argued by Traub and Berk [15] that a steady laminar shear stress "promotes release of factors from endothelial cells that inhibit coagulation, migration of leukocytes, and smooth muscle proliferation while simultaneously promoting cell survival." On the other hand, "low shear stress and flow reversal shift the profile of secreted factors and expressed surface molecules to one that favors opposite effects." Berry et al. [14] have shown that vortices developed due to struts may enhance platelet activation and may also affect the ability of the endothelial cells to regrow over the stented region. Wentzel et al. [16,17] have conducted clinical studies and shown that neointimal formation was pronounced when the shear stress was low while it was reduced at higher shear stress levels. LaDisa et al. [18] have computed the flow through a three dimensional stented vessel and found that the WSS decreases by 77% in a stented vessel compared to a stent-free vessel. Rajamohan et al. [19] have computed the pulsating flow in a three-dimensional stented vessel and determined that regions of low and negative WSS represent locations of thrombus formation and platelet accumulation.

Caution seems to be necessary when one considers drug eluting stents. The study by Brinda Balakrishnan et al. [7] shows that the mechanism of recirculation can, in fact, help a good drug deposition. Their study indicates that more drug is deposited by fluid mediated transport than by actual contact. Our considerations naturally exclude the drug eluting stents.

Literature reveals that the width, thickness, and spacing of the struts of the stent control the shear stress and recirculation of flow. The effect of these parameters has been studied in detail by Seo et al. [9]. The length of the recirculation zone downstream of the stent increases with the Reynolds number of flow (based on inlet velocity and vessel diameter) and with stent diameter, but weakly depends on strut spacing. However, the recirculation in between the struts is found to be strongly dependent on strut spacing. Berry et al. [20] have studied the effect of strut spacing upon hemodynamics with the aid of flow visualization by injecting dyes and with computations. They have found a significant deposition of

[1]Corresponding Author. Permanent address: School of Aerospace, Mechanical and Mechatronic Engineering, University of Sydney, NSW 2006, Australia.

Manuscript received February 27, 2007; final manuscript received January 29, 2008; published online March 10, 2008. Review conducted by James Moore

dye when the strut spacing was about three wire diameters while a spacing of six diameters was the optimum. Moore and Berry [21] and Frank et al. [5] have conducted their investigations on strut spacing with computational fluid dynamics and determined that the platelet deposition increases with recirculation of flow, which in turn increases with strut spacing. Similar conclusions have also been reached by Duraiswamy et al. [22], while Kasrati et al. [23] have found that a thinner strut produces a substantially lower restenosis than a thick strut.

The natural questions that arise are as follows. Has there been any attempt to optimize the design of a stent to avoid restenosis? Have hemodynamic processes been taken into account? The answer seems to be negative. The only exception seems to be the work of Tesch et al. [24], who have used the evolutionary algorithms (EAs) (which do include the genetic algorithms (GAs) [25]) for optimization. Such methods are known to be very time consuming.

In this work, we have formulated objective functions to reflect the requirement discussed above, namely, the WSS does not reach low values and the recirculation zone has to be a minimum. Then, we have carried out an optimization based on the modern principles of design, namely, exploration of design space [26]. Some of the assumptions that set the limits of this work are as follows. The objective functions used in this work were computed for a steady, two-dimensional flow of blood. A model stent with three struts was considered. For the present work, the flow Reynolds number based on inlet conditions was chosen to be 400. Furthermore blood was considered Newtonian with a density of 1060 kg/m^3 and a viscosity of 0.0035 kg/m s [9]. Blood is typically non-Newtonian in character. However, it has been shown that this is true mainly when the shear rates are smaller than 100/s [27]. Such shear rates may occur within the recirculation zones in a stented flow. However, the computations by Seo et al. [9] have shown that while considering blood as non-Newtonian, the length of the recirculation zone is reduced only by about 8%. Consequently, it was decided to treat blood as Newtonian in the present work. Then, in reality, the blood flow is pulsating. Again, the results of Seo et al. [9] clearly demonstrate that the peak value of the recirculation length computed for a pulsating flow matches that for the steady flow. Furthermore, in the present optimization schedule, we need to perform a number of computations, 60 for each test case, and time requirement would be enormous for a pulsating flow. For optimization purposes, a steady flow calculation is considered sufficient.

The details of the method of optimization are given later in the paper. We may also point out that the present work distinguishes itself from any of the computational studies of the past. Our work is one of optimization of design based on computations and attempts to take a step forward toward evolving a better stent.

2 Method

In the spirit of the method used, namely, exploration of design space, one examines a large number of candidate designs and evolves an optimum. The first step is to select these candidates, which in the present work was carried out using Latin hypercube sampling [28]. This is basically a statistical method, which attempts to generate a plausible collection of parameter values (design variables) from a multidimensional distribution. Effectively, it reduces the number of trials one has to perform, which in our case will be the number of samples to consider. In this work, we choose 60 samples. The next step is to evaluate the fitness or the objective functions for each of these samples through experiments or computations. We have followed the latter approach and used the commercial software FLUENT for the purpose. The details of computation are given later in this section. This was followed by the process of Kriging [29], to produce a response surface [30], which represents the relationship between the objective functions and the design variables. Kriging essentially predicts unknown (optimum) values from the data collected with experiments (computations in our case). The procedure also yields what are called *nondominated solutions*. These contain several optimized solutions, allowing the designer to select the one that suits a given situation. For the present work, an in-house software was used for Latin hypercube sampling and Kriging.

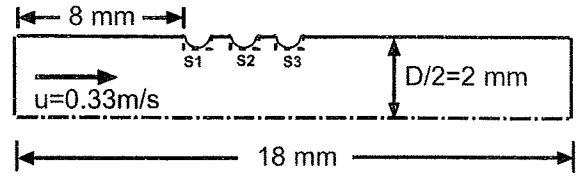

Fig. 1 Geometry of the test case

2.1 Objective Functions. We have considered a stent with three struts, S1, S2, and S3, either of semicircular cross section or of rectangular cross section, as shown in Fig. 1. The number of struts was fixed to be 3 following the work of Seo et al. [9], where it is shown that the size of the recirculation zone downstream of the stent decreases as the number of struts increases. However, the decrease is not appreciable for strut numbers greater than 3. The objectives considered are as follows.

(a) Following the studies reviewed before, it is clear that the recirculation zone both downstream of the stents and in the region between the struts is to be minimized. In the present work, we have considered as one objective, L, the length of the recirculation zone past strut S3, as shown in Fig. 2. For each of the 60 cases, this was determined by plotting the streamlines and locating the recirculation zone.

(b) Minimization of recirculation alone may not be sufficient from the point of view of neointimal hyperplasia [14]. An appreciable reattachment of flow is also desired in between the struts. Accordingly, a second objective was also introduced in the present study, namely, DR, the reattachment distance past strut S1 also sketched in Fig. 2. This distance was measured by drawing the velocity vector and streamline plots for each of the 60 samples and measuring the reattachment distance in pixels. To be used as one of the objective functions, this was later expressed as a percentage of the spacing in between the struts (DS1S2) i.e.,

$$\mathrm{RDI} = \frac{\mathrm{DR}}{\mathrm{DS1S2}} \times 100 \tag{1}$$

This objective is to be maximized.

(c) It may be noted that recirculation of flow and reattachment are typical viscous effects. One method of quantifying them is to compute $D\omega$, the additional vorticity generated by the stent. Minimization of this could result in a control of viscous effects. Accordingly, we choose $D\omega$ as one of the primary objective functions to be minimized, but express it as a percentage of vorticity in the unstented vessel. Vorticity is obtained by integrating the computed velocity field, a feature readily available in FLUENT and that generated by stent was determined by

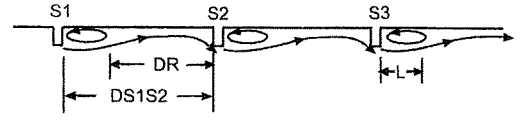

Fig. 2 Schematic showing length of recirculation zone L and reattachment distance DR

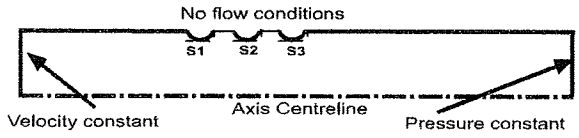

Fig. 3 Boundary conditions for computation

calculating vorticity in the flow field first without stent and then with the stent. The difference was considered as the vorticity generated by stents. Expressions for vorticity generated and the exact objective function used are as follows.

$$D\omega = \int_S \nabla \times \mathbf{V} - \int_{NS} \nabla \times \mathbf{V} \tag{2}$$

$$\Delta\omega = \frac{D\omega}{\int_{NS} \nabla \times \mathbf{V}} \times 100 \tag{3}$$

where $\mathbf{V}$ is the velocity vector, subscript S refers to a stented vessel, and NS refers to an unstented vessel.

2.2 Test Cases. Two test cases, both involving a two-dimensional axisymmetric flow in a 4 mm diameter and 18 mm long vessel, as shown in Fig. 1, were considered. The first one was of semicircular cross section, while the second one was rectangular in cross section.

2.3 Computation of Flow Field and Objective Functions. Objective functions for each of the cases were computed under the assumptions stated earlier. The boundary conditions used, shown in Fig. 3, were the standard ones—constant velocity conditions at the entry, constant pressure conditions at the exit, axis conditions on the centerline, and no flow conditions on the solid walls.

The flow was computed using the supercomputer available at the Tohoku University.

At the beginning of computations, runs were carried out for some of the typical cases considered by Seo et al. [9] and confirmed that we also obtain similar results.

3 Results

3.1 Test Case 1, Semicircular Cross Section. For the present test case with semicircular cross section, the design variables were d, the diameter of the strut, and w, the spacing of the strut, while the depth t is given by $d/2$. The range of design variables was determined from an inspection of the available stents and is shown in Table. 1 with reference to Fig. 4.

3.1.1 Objective Functions for Optimization. After computing the 60 cases, it was found that for the range of design variables considered, there was no recirculation of flow either after the stent or in between the struts for the semicircular stents. Only local negative velocities were noticed in some cases. Then, it was decided to replace this objective (a) given in Sec. 2.1 with the minimum shear stress past the third strut, S3, which was to be maximized. The two objective functions considered for this case were as follows:

(a) Vorticity generated due to stents be a minimum, $\Delta\omega$ (Eq. (3)).

(b) The magnitude of minimum WSS past the third strut, S3, to be a maximum. This is given by the expression

$$\tau = \mu\left(\frac{\partial u}{\partial y} + \frac{\partial v}{\partial x}\right)_{\text{wall}} \tag{4}$$

and is available readily as an output with the software FLUENT. Following computations, shear stress distribution along the wall was plotted for each of the cases. The minimum point downstream of S3 was located and the corresponding shear stress was taken as the objective

Table 1 Range of design variables for the stent with semicircular struts

Variables	Range
d/D	0.01–0.1
w/D	0–0.6

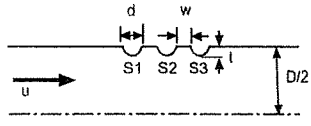

Fig. 4 Geometry of stent with semicircular struts

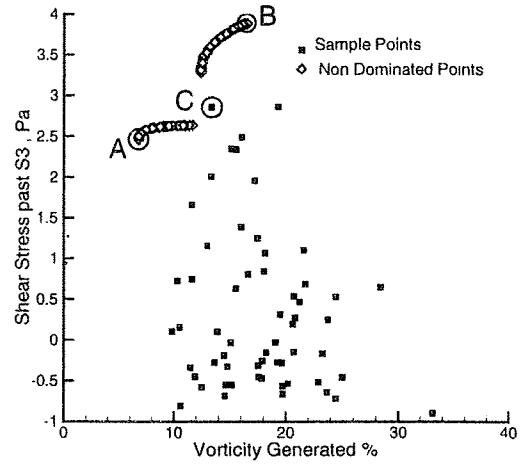

Fig. 5 Nondominated front for stent with semicircular struts. Stent *A* has least vorticity, *B* has highest shear stress past S3, and *C* is a compromise stent.

3.1.2 Results for the Stent of Semicircular Cross Section. Computational grid was generated for each of the samples consisting of approximately 13,000 triangular elements. The flow field was computed using FLUENT and the two objective functions were evaluated. Each case took less than a minute of CPU time on the supercomputer. It was found that vorticity generated ranged from a minimum of 0.1974 m^2/s to a maximum of 0.9659 m^2/s, while the shear stress ranged from −0.895 Pa to 2.86 Pa. The magnitude of shear stress upstream of the stent was around 5 Pa.

The evaluated objective function values and the corresponding design variables were processed by a Kriging software to yield a response surface from which the nondominated members were identified. The outcome is shown in Fig. 5 where the objective functions are plotted in a space defined by the two objectives: vorticity generated (expressed as a percentage of that for the non-stented vessel) and the minimum WSS past the strut, S3. Each of the nondominated points represents a stent and is one of the acceptable designs. The designer can now make a selection of the best stent. If one is after a stent which generates least amount of vorticity, the choice will be A. For the shear stress consideration, it will be B. Many compromise designs exist between A and B. We select one, C, which is approximately midway in between the two and forms the compromise stent in the present case. The values of the design variables for A–C are given in Table 2, where $\Delta\omega$

Table 2 Optimized stents with semicircular struts, ND indicates nondominated

	A 0.0293, 0.284		*B* 0.0110, 0.0977		*C* 0.0235, 0.271	
d/D, w/D=	ND	Realized	ND	Realized	ND	Realized
$\Delta\omega$ (%)	6.79	6.76	15.9	18.29	11.67	15.98
τ (Pa)	2.46	2.49	3.86	3.36	2.64	2.69

stands for the vorticity generated and τ is the shear stress.

For verification purposes, the calculation of objectives was repeated for the identified cases, $A-C$, by computing them in the usual manner. Table 2 shows the predicted as well as the realized values of the objective functions; most of the predictions are realized. From shear stress considerations, it seems better to have the design variables at their lower limit.

The streamlines for the three identified cases are shown in Fig. 6. Absence of flow recirculation is evident in each of the three cases. The WSS distribution for these stents is shown in Fig. 7.

3.2 Test Case 2, Rectangular Cross Section. The range of design variables for this case is given in Table 3 with reference to Fig. 8. The grid and the boundary conditions used were similar to those for the semicircular case. It was found that vorticity generated ranged from a minimum of 0.401 m^2/s to a maximum of 1.773 m^2/s, while the length of recirculation zone ranged from 0.272 mm to 1.953 mm and the reattachment distance was between 0% and 60% of the strut spacing. Two nondominated fronts were obtained:

(a) one in vorticity-recirculation distance space, $\Delta\omega-L$

(b) the second one in vorticity-reattachment distance, $\Delta\omega$ −RDI, space

The nondominated fronts are shown in Figs. 9 and 10. The results are tabulated in Tables 4 and 5, where $\Delta\omega$ is the vorticity generated. L is the length of the recirculation zone, and RDI is the reattachment distance expressed as a percentage of strut spacing.

We can identify three nondominated designs, *A*, *B*, and *C*, from Fig. 9, which are minimum vorticity, minimum recirculation length, and the compromise stents, respectively. As expected, the present optimization prefers the minimum possible thickness and a maximum possible width for the stent. Regarding spacing, there seems to be no preference. However, when one looks at the nondominated designs *D*, *E*, and *F* from Fig. 10 (being minimum vorticity, maximum reattachment length, and compromise stents, respectively), it is clear that the interstrut spacing should be large (7*d*, 15*d*, and 11*d*, respectively). This finding is in close agree-

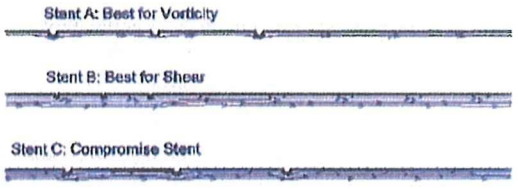

Fig. 6 Streamlines in region of interest for stents with semicirculat struts, *A–C*; note the absence of recirculation in each of them

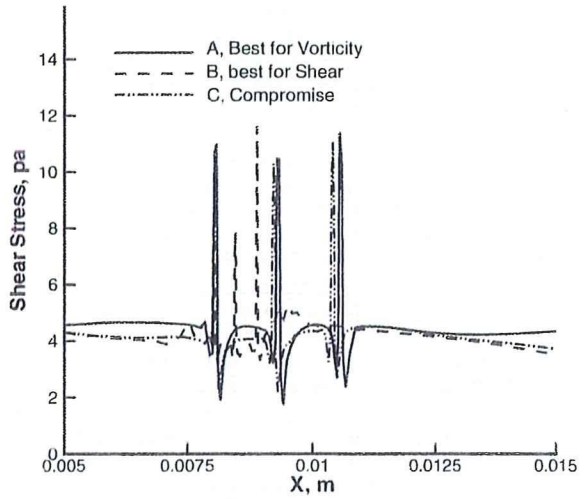

Fig. 7 Comparison of shear stress past the stents with semicircular struts. Shear stress past S3 is highest for *B*

Table 3 Range of design variables for stent with rectangular struts

Variable	Range
d/D	0.01–0.1
w/D	0–0.6
t/D	0.05–0.1

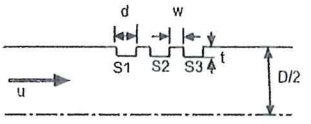

Fig. 8 Geometry of stent with rectangular struts

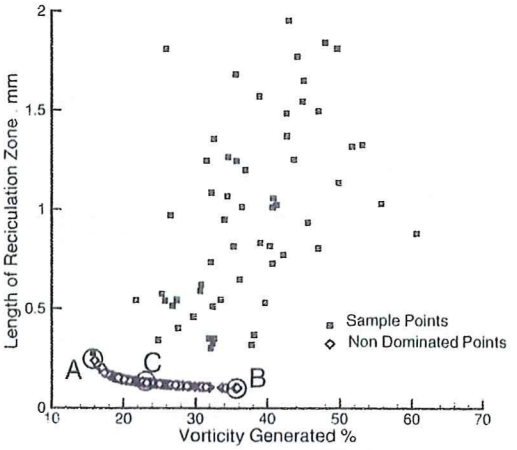

Fig. 9 Nondominated front in $\Delta\omega-L$ space for stent with rectangular struts. *A* has least vorticity, *B* has the least recirculation length, and *C* is a compromise stent.

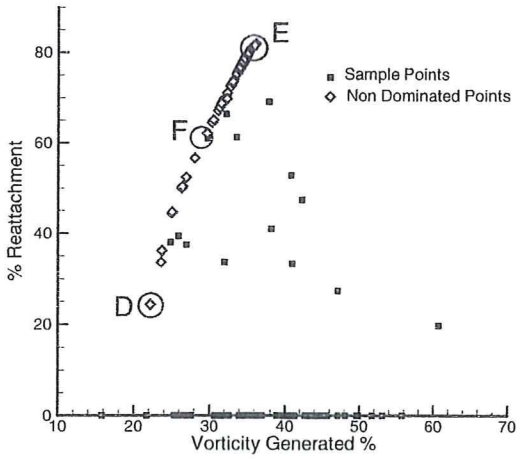

Fig. 10 Nondominated front in $\Delta\omega$-RDI space for stent with rectangular struts. *D* has least vorticity, *E* has the highest reattachment length, and *F* is a compromise stent.

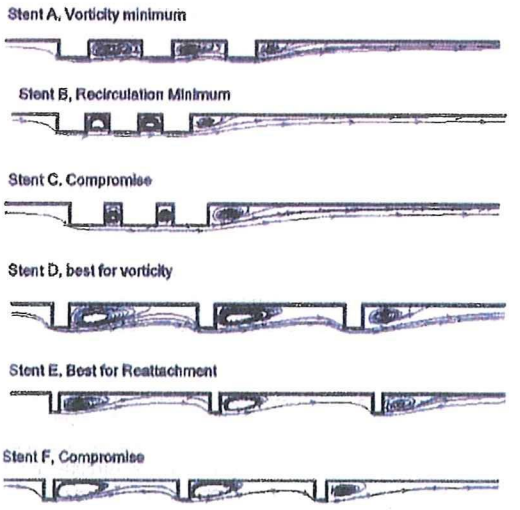

Fig. 11 Streamlines in region of interest for stents with rectangular struts, *A–F*

ment with the results of Berry et al. [14] and Kastrati et al. [23] that for reattachment downstream of a wire, the spacing should be at least six times the diameter of the wire. The streamline plots for cases $A-F$ are given in Fig. 11 from which it is clear that there is a recirculating flow both downstream of the stent and also in between the struts.

4 Discussion

First, we compare the predicted (nondominated) and realized values of objective functions for the two test cases. Considering vorticity generated, in general, there is a good agreement; sometimes, the realized values are better than predicted. This is to be expected as vorticity generated is an integrated quantity. However, the length of recirculation zone L and the reattachment distance RDI are very specific quantities and are dependent on many features of the flow. It is not unexpected that, sometimes, the recirculation zone seems longer than that predicted, whereas the reattachment distance is smaller than predicted. We have to note that we are more after an optimum design than a close agreement between the two solutions. Shear stress, on the other hand, exhibits a better agreement.

Many observations significant from a medical point of view could be made from the results of optimization shown in the previous sections. First of all, it appears better to use a semicircular section for the strut than a rectangular section. A semicircular strut whose dimensions are within the design limits ensures that there is no recirculation of flow downstream of the stent. Furthermore, the optimized stent clearly has no recirculation in between the struts as well.

For stents of rectangular cross section, a minimum thickness close to 0.055 of the vessel diameter and a width close to 0.1 of the vessel diameter seem to be optimal. If a considerable reattached flow is desired in the region in between the struts, the spacing w is to be increased sufficiently (almost to ten times the width of the strut). It is worth comparing our results with the dimensions of some of the available stents. Table 6 shows such a comparison. Clearly, the dimensions of the optimum stent are closer to those of the COOK stent (measurements were made in house for this stent). For the other stents, we have obtained the thicknesses from Ref. [31]. It appears that these designs are conservative regarding thickness.

It should be noted that the results of optimization are strictly valid for the conditions for which the objective functions have been evaluated. There is a good possibility that change of flow conditions leads to a different result. The applicability of the re-

Table 4 Results for stents with rectangular struts in vorticity and recirculation length space, ND indicates nondominated

	A 0.0981, 0.173, 0.0546		*B* 0.0888, 0.0686, 0.0556		*C* 0.0943, 0.0437, 0.0559	
d/D, w/D, t/D=	ND	Realized	ND	Realized	ND	Realized
$\Delta\omega$ (%)	16.03	14.96	35.8	14.68	25.8	16.46
L (mm)	0.24	0.272	0.1	0.27	0.12	0.335

Table 5 Results for optimization of stent with rectangular struts in vorticity and reattachment length space, ND indicates nondominated

	D 0.0431, 0.313, 0.0568		*E* 0.0288, 0.456, 0.0568		*F* 0.0329, 0.375, 0.0569	
d/D, w/D, t/D=	ND	Realized	ND	Realized	ND	Realized
$\Delta\omega$ (%)	22.16	35.77	36.1	29.44	29.6	35.63
RDI (%)	24.39	29.6	82.0	59.0	62.1	46.0

Table 6 Dimensions of some of the commercially available stents

Stent	Manufacturer	Dimensions		
		d/D	w/D	t/D
COOK	COOK Inc.	0.02275	0.6535	0.016
JJIS coronary	Johnson and Johnson			0.0187
JJIS biliary	Johnson and Johnson			0.0373
Multilink	Advanced Cardiovascular Systems			0.0149
Navius ZR1	Navius			0.0067
Present (semicircular, C)		0.0235	0.271	0.0117
Present (rectangular, C)		0.0943	0.0437	0.0559
Present (rectangular, F)		0.0329	0.375	0.0569

sults for a different set of conditions will depend on the sensitivity of the objective functions for the chosen flow conditions. For example, it has been assumed here that the strut is placed at right angles to the main flow. The results may not be directly applicable when this assumption is violated or in the presence of three-dimensional effects. Furthermore, we note that the stent behavior is influenced by many factors apart from structural strength, material properties, cell properties, etc. A real design has to account for all these influences or effects. In addition, the discipline of optimization has today developed to such an extent that it is indeed possible to include inputs from all the fields listed above. We have started an ambitious program wherein we wish to optimize the design of stent in such a truly multidisciplinary approach. Such a work has to be three dimensional and is complicated. In the present paper, which may be regarded as the first step, we restrict ourselves to a two-dimensional approach wherein we address some of the broad design features of stents. The real life cases of optimization will be considered in our future work.

5 Conclusion

Design optimization has been performed on coronary stents with semicircular and rectangular struts using the modern principle of exploration of design space. During optimization vorticity generated by the stent, the length of the recirculation zone downstream of the stent was minimized, while the reattachment length after the first strut was maximized. The optimized values of strut width, thickness, and spacing are comparable to the ones found in some of the commercially available stents. A three-dimensional multi disciplinary optimization considering inputs from various disciplines will be considered in future.

Acknowledgment

We thank the reviewers for an objective criticism of the first two versions of the paper. We also acknowledge the help of Joel Tenne, Lym Jin Ne, Takayasu Kumano, and Shinkyu Jeong from the Institute of Fluid Science, Tohoku University, during the course of this work.

Nomenclature

D = diameter of the vessel
DR = reattachment distance downstream of Strut S1
DS1S2 = distance between Struts S1 and S2
$D\omega$ = vorticity generated by the stent
L = the length of recirculation zone downstream of the stent
RDI = DR expressed as a percentage of DS1S2
S1 = Strut 1
S2 = Strut 2
S3 = Strut 3
$\mathbf{V}$ = velocity vector
X = distance along the x coordinate
d = diameter of semicircular strut, width of rectangular strut
t = thickness of strut (=$d/2$ in the case of semicircular strut)
u,v = velocities in the x and y directions
w = spacing between the struts
x,y = distances in the x and y directions
μ = viscosity
τ = shear stress
ω = vorticity=$\nabla \times \mathbf{V}$
$\Delta\omega$ = vorticity generated by the stent expressed as a percentage

Subscripts

S = stented vessel
NS = nonstented vessel

References

[1] Grewe, P. H., Deneke, T., Machraoui, A., Barmeyer, J., and Müller, K. M., 2000, "Acute and Chronic Tissue Response to Coronary Stent Implantation: Pathologic Findings in Human Specimen," J. Am. Coll. Cardiol., **35**, pp. 157–163.

[2] Lemos, P. A., Serruys, P. W., and Sousa, J. E., 2003, "Drug-Eluting Stents: Cost Versus Clinical Benefit," Circulation, **107**, pp. 3003–3007.

[3] Lally, C., Dolan, F., and Prendergast, P. J., 2005, "Cardiovascular Stent Design and Vessel Stresses: A Finite Element Analysis," J. Biomech., **38**, pp. 1574–1581.

[4] Kastrati, A., Mehili, J., Dirschinger, J., Pache, J., Ulm, K., Schuhlen, H., Seyfarth, M., Schmitt, C., Blasini, R., Neumann, F.-J., and Schomig, A., 2001, "Restenosis After Coronary Placement of Various Stent Types," Am. J. Cardiol., **87**, pp. 34–39.

[5] Frank, A. O., Walsh, P. W., and Moore, Jr., J. E., 2002, "Computational Fluid Dynamics and Stent Design," Artif. Organs, **26**(7), pp. 614–621.

[6] Lowe, H. C., Oesterle, S. N., and Khachigian, L. M., 2002, "Coronary In-Stent Restenosis: Current Status and Future Strategies," J. Am. Coll. Cardiol., **39**, pp. 183–193.

[7] Brinda Balakrishnan, S. B., Tzafriri, A. R., Seifert, P., Groothius, A., Rogers, C., and Edelman, E. R., 2005, "Strut Position, Blood Flow and Drug Deposition. Implications for Single and Overlapping Drug-Eluting Stents," Circulation, **111**, pp. 2958–2965.

[8] Benard, N., Perrault, R., and Coisne, D., 2006, "Computational Approach to Estimating the Effects of Blood Properties on Changes in Intra-Stent Flow," Ann. Biomed. Eng., **34**(8), pp. 1259–1271.

[9] Seo, T., Schachter, L. G., and Barakat, A. L., 2005, "Computational Study of Fluid Mechanical Disturbance Induced by Endovascular Stents," Ann. Biomed. Eng., **33**, pp. 444–456.

[10] Stuhne, G. R., and Steinman, D. A., 2004, "Finite Element Modeling of the Hemodynamics of Stented Aneurysms," ASME J. Biomech. Eng., **126**, pp. 382–387.

[11] Nakayama, T., Ohta, M., Rufenacht, D. A., and Takahashi, A., 2007, "The Effect of Stenting With Difference Positions on Hemodynamics in a Cerebral Aneurysm," *The Ninth International Symposium on Future Medical Engineering Based on Bio-Nanotechnology*, Tohoku University 21st Century COE Programme, Jan. 7–9, Sendai International Center, Sendai, Japan, pp. 106–107.

[12] Cebral, J. R., Castro, M. A., Burgess, J. E., Pergolizzi, R. S., Sheridan, M. J., and Putman, C. M., 2005, "Characterization of Cerebral Aneurysms for Assessing Risk of Rupture by Using Patient Specific Computational Hemodynamics Models," AJNR Am. J. Neuroradiol., **26**, pp. 2550–2559.

[13] Whittaker, D. R., and Fillinger, M. F., 2006, "The Engineering of Endovascular Stent Technology: A Review," Eur. J. Vasc. Endovasc. Surg., **40**(2), pp. 85–94.

[14] Berry, J. L., Moore, J. E., Newman, V. S., and Routh, W. D., 1997, "In Vitro Flow Visualization in Stented Arterial Segments," J. Vasc. Invest., **3**, pp. 63–68.

[15] Traub, O., and Berk, C. B., 1998, "Laminar Shear Stress: Mechanisms by

which Endothelial Cells Transduce an Atheroprotective Force," Ann. Allergy Asthma Immunol., **18**, pp. 677–685.
[16] Wentzel, J. J., Whelan, D. M., van der Giessen, W. J., van Beusekom, H. M. M., Andhyiswara, I., Serruys, P. W., Slager, C. J., and Krams, R., 2000, "Coronary Stent Implantation Changes 3-D Vessel Geometry and 3-D Shear Stress Distribution," J. Biomech., **33**, pp. 1287–1295
[17] Wentzel, J. J., Krams, R., Schuurbiers, J. C., Oomen, J. A., Kloet, J., van Der Giessen, W. J., Serruys, P. W., and Slager, C. J., 2001, "Relationship Between Neointimal Thickness and Shear Stress After Wall Stent Implantation in Human Coronary Arteries," Circulation, **103**, pp. 1740–1745.
[18] LaDisa, Jr., J. F., Guler, I., Olson, L. E., Hettrick, D. A., Kersten, J. R., Warltier, D. C., and Pagel, P. S., 2003, "Three-Dimensional Computational Fluid Dynamics Modeling of Alterations in Coronary Wall Shear Stress Produced by Stent Implantation," Ann. Biomed. Eng., **31**, pp. 972–980.
[19] Rajamohan, D., Banerjee, R. K., Back, L. H., Ibrahim, A. A., and Jog, M. A., 2006, "Developing Pulsatile Flow in a Deployed Coronary Stent," ASME J. Biomech. Eng., **128**, pp. 347–359.
[20] Berry, J. L., Santamarina, A., Moore, Jr., J. E., Roychowdhury, S., and Routh, W. D., 2000, "Experimental and Computational Flow Evaluation of Coronary Stents," Ann. Biomed. Eng., **28**, pp. 386–398.
[21] Moore, J. E., and Berry, J. L., 2002, "Fluid and Solid Mechanical Implications of Vascular Stenting," Ann. Biomed. Eng., **30**, pp. 1–11.
[22] Duraiswamy, N., Jayachandran, B., Byrne, J., Moore, Jr., J. E., and Schoephoerster, R. T., 2005, "Spatial Distribution of Platelet Deposition in Stented Arterial Models Under Physiologic Flow," Ann. Biomed. Eng., **33**(12), pp. 1767–1777
[23] Kastrati, A., Mehilli, J., Dirschinger, J., Dotzer, F., Schühlen, H., Neumann, F.-J., Fleckenstein, M., Pfafferott, C., Seyfarth, M., and Schömig, A., 2001, "Intracoronary Stenting and Angiographic Results: Strut Thickness Effect on Restenosis Outcome (ISAR-STEREO) Trial," Circulation, **103**, pp. 2816–2821
[24] Tesch, K., Atherton, M. A., and Collins, M. W., 2002, "Genetic Algorithm Search for Stent Design Improvements," *Proceedings of the Fifth International Conference on Adaptive Computing in Design and Manufacture*, Apr. 16–18, University of Exeter, Devon, UK, pp. 99–107.
[25] Goldberg, D. E., 1989, *Genetic Algorithms in Search, Optimization and Machine Learning*, Addison-Wesley, Reading, MA.
[26] Jeong, S., and Obayashi, S., 2006, "Multi-Objective Optimization Using Kriging Model and Data Mining," KSAS International Journal, **7**, pp. 1–12.
[27] Chien, S. S., Usami, S., Taylor, M., Lundenburg, J. L., and Gergersem, M. I., 1966, "Effects of Hematocrit and Plasma Proteins on Human Blood Rheology at Low Shear Rates," J. Appl. Physiol., **21**, pp. 81–87
[28] Mckay, M. D., Beckman, R. J., and Conover, W. J., 1979, "A Comparison of Three Methods for Selecting Values of Input Variables in the Analysis of Output From a Computer Code," Technometrics, **21**(2), 239–245
[29] Donald, R. J., Matthias, S., and William, J. W., 1998, "Efficient Global Optimization of Expensive Black-Box Function," J. Global Optim., **13**, pp. 455–492.
[30] Myers, R. H., and Montgomery, D. C., 1995, *Response Surface Methodology: Process and Product Optimization Using Designed Experiments*, Wiley, New York, pp. 1–84.
[31] Yamamoto, Y., Brown, D. L., Ischinger, T. A., Arbab-Zadeh, A., and Penny, W. F., 1999, "Effect of Stent Design on Reduction of Elastic Recoil: A Comparison via Quantitative Intravascular Ultrasound," Catheterization and Cardiovascular Interventions, **47**(2), pp. 251–257.

Three-Dimensional Reconstruction of a Cerebral Stent using Micro-CT for Computational Simulation

Makoto Ohta, Chuan He, Toshio Nakayama, Akira Takahashi and Daniel A. Rüfenacht

Journal of Intelligent Material Systems and Structures 2008; 19; 313 originally published online Dec 21, 2007;
DOI: 10.1177/1045389X07083184

Three-Dimensional Reconstruction of a Cerebral Stent using Micro-CT for Computational Simulation

MAKOTO OHTA,[1,*] CHUAN HE,[2] TOSHIO NAKAYAMA,[1] AKIRA TAKAHASHI[2] AND DANIEL A. RÜFENACHT[3]

[1]*Institute of Fluid Science, Tohoku University, 2-1-1 Katahira, Aoba-ku, Sendai, 980-8577, Japan*

[2]*Department of Neuroendovascular Therapy, Tohoku University, 2-1 Seiryo-machi, Aoba-ku, Sendai, 980-8575 Japan*

[3]*Department of Neuroradiology, Geneva University Hospital, Rue Micheli-du-Crest 24, Geneva, 1211, Switzerland*

ABSTRACT: The surface geometry of an intracranial stent (ICS) for a cerebral aneurysm is reconstructed by using micro-CT to import computational fluid simulations. The reconstructed stent with STL format is composed of 170,948 triangles with 0.04 mm spatial resolutions. The boundary condition of the surface is clear without any reflection effects by X-ray introduced into the stainless steel stent. The computational simulations of blood flow with small implants, such as a stent or coil will be a designable way to control blood flow in/on a cerebral aneurysm and repair the disease. Micro-CT has a possibility of detecting the 3-D geometry of a small implant, such as ICS and may be useful to 3-D reconstruction and integration to computational simulation.

Key Words: stent, cerebral aneurysm, micro-CT, CFD.

INTRODUCTION

IMAGE guided minimally invasive treatments (IGMIT) is an endovascular treatment using catheters and micro guide wires on a digital subtraction angiography (DSA). Recent studies have reported that endovascular treatments have a possibility of repairing cerebral aneurysms using implantation, such as a coil or stent (Molyneux et al., 2002; Fiorella et al., 2004). These implants have the potential to repair diseases by decreasing blood flow in the cavity. Aenis et al. (1997) using finite element method (FEM) on a hexagonal mesh to model flow past stent struts aligned perpendicular to the parent artery, found a decrease in flow speed in the aneurysm after stenting. Hirabayashi et al. (2003) characterized the effect of stent position on flow speed by using Lattice-Boltzmann method, identifying positioning of the stent struts to have an influence on the flow speed. Ohta et al. (2004b) assumed the stent struts to be two parallel sticks and investigated the flow pattern on the neck using FEM. These reports use idealized geometries of an aneurysm and stent.

An intracranial stent (ICS) is made of stainless steel or NiTi (Yoshida et al., 1991). The former is expanded by a balloon and called the balloon expandable stent and the latter is expanded by a shape memory effect and called the self-expandable stent. The stent design is based on braided or laser cut, therefore, it is difficult to predict the stent geometry after the expansion and is important to measure the geometry to import the computational simulation.

The techniques of three-dimensional (3-D) reconstructions based on patient geometry from sliced images of computed tomography (CT), DSA, or magnetic resonance images (MRI) have been developed for decades. The medical imaging equipment allows reconstructing 3-D geometries by a rotational mechanism and exported sliced images (3-D sliced digital imaging and communications in medicine (DICOM)) or 3-D surface meshing format, such as the stereolithography (STL) or virtual reality modeling language (VRML). This method has been used for a computational simulation of blood flow in aneurysms to investigate the impact of the flow on the generation, growth, or rupture of the aneurysm (Hassan et al., 2003; Steinman et al., 2003; Cebral et al., 2005, Shojima et al., 2005). The 3-D data are also used for biomodeling from rapid prototyping to develop *in vitro* experiments (D'Urso et al., 1999; Ohta et al., 2004a; Wetzel et al., 2005). However, the spatial resolution of the conventional medical imaging equipment is around 150 μm to 1 mm. The stent strut is from around 20 to 100 μm, so that it was difficult to reconstruct the geometry by the conventional medical imaging equipment.

*Author to whom correspondence should be addressed.
E-mail: ota@imail.ifs.tohoku.ac.jp
Figures 1–3 and 5–8 appear in color online: http://jim.sagepub.com

1045-389X/08/03 0313–6 $10.00/0 DOI: 10.1177/1045389X07083184

Micro-CT is one of the potential tools for 3-D reconstruction of the small implants and converting STL files for importing computational simulations due to the high spatial resolution. Jiang et al. (2000) used it for trabecular geometry, and Langheinrich et al. (2005) used it as the diagnosis method after stenting into stenosis. Cheema et al. (2006) delineated adventitial microvessel using micro-CT. He et al. (2006) applied micro-CT for measuring blood flow of rat as an angiography. These results exhibit micro-CT useful for measuring geometry of small samples. However, there are no reports of using the geometries as computational simulation, such as blood flow in an aneurysm.

In this study, the authors measure the geometry of ICS before and after the expansion to find the possibility to be useful to the computational simulation.

MATERIALS AND METHODS

3-D Reconstructions of ICS by Micro-CT

An ICS (INX, Medtronic) was made of stainless steel on a balloon system. After setting it up in Microfocus X-ray Television System (SMX-100CT, Shimadzu Corporation) as shown in Figure 1, the stent was expanded by injecting water into the balloon using a syringe. The X-ray with 60 kV and 40 μA was induced to the stent in $5.76 \times 5.76 \times 4.77\,mm^3$ as field of view (FOV).

The micro-CT exported sliced files composed of 512×512 pixels and 0.04 mm thickness with tagged image file format (TIFF) and the sliced files were imported into Mimics (7.30, Materialise) to perform a 3-D reconstruction with STL format. The stent geometry was merged into a patient on Magics (8.0, Materialise).

3-D Reconstructions of ICS from Computed Aided Design

To compare with the ICS geometry based on micro-CT, a stent strut was constructed by computed aided design (CAD) techniques with Pro/Enginnering (6.5). The six tops around the circle constructed the struts and the rectangle formed the surface.

3-D Reconstructions of a Cerebral Aneurysm from Patient Data

The angiographical data of a 43-year-old female patient with an unruptured ophthalmic internal carotid artery aneurysm on the left side were acquired by rotational digital subtraction angiography (3D-RA, BV 3000, Philips Medical Systems (PMS)) prior to medical treatment. The raw data consisting of 100 views were obtained during a rapid rotational movement of the C-arm based X-Ray equipment. During the movement of C-arm, the contrast media (Iopamiro 300, BRACCO SUISSE S. A.) was injected at 3 mL/s into the parent artery near to the aneurysm. The C-arm movement was performed for 180° and 8 s at 12.5 frames/s with 17–30 cm FOV and 1024×1024 matrixes. The data were transferred to a 3-D post-processing workstation (INTEGRIS 3D-RA release 2.2, PMS). Three-dimensional reconstructions of the internal carotid artery injection were displayed and saved in virtual reality modeling language (VRML) format (Cardio-Vascular Department, customer requested adaptation, PMS). The VRML file was imported into Magics via GLview (free software package).

RESULTS

Figure 2 shows an example of the fluoroscopic image of the stent after expanding and Figure 3 shows the 3-D reconstruction where the white is the stent struts and the reflection from the struts is found in and out of the stent.

After selecting a proper threshold of white and black balance in the sliced images, the 3-D reconstruction with a binary picture is shown in Figure 4. The stent struts are clear and enough to recognize the boundary (stent surface) without any noisy reflection.

Figure 5 shows the 3-D reconstruction after converting to STL format in (a) and the triangles in (b).

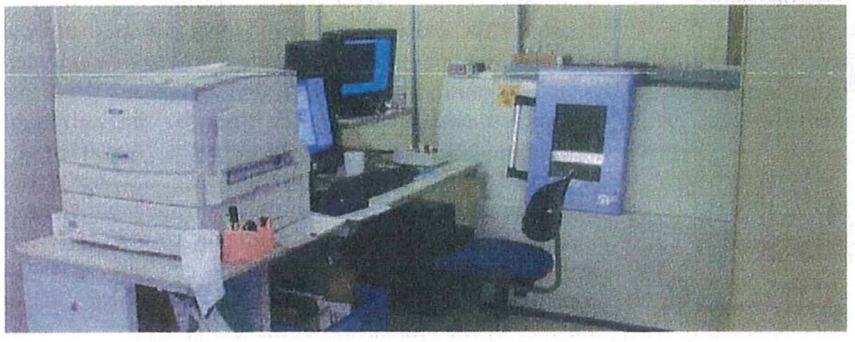

Figure 1. Microfocus X-ray television system (SMX-100CT, Shimadzu Corporation).

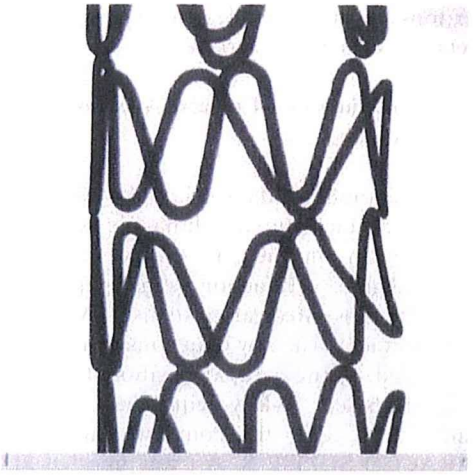

Figure 2. *An example of fluoroscopic image of ICS.*

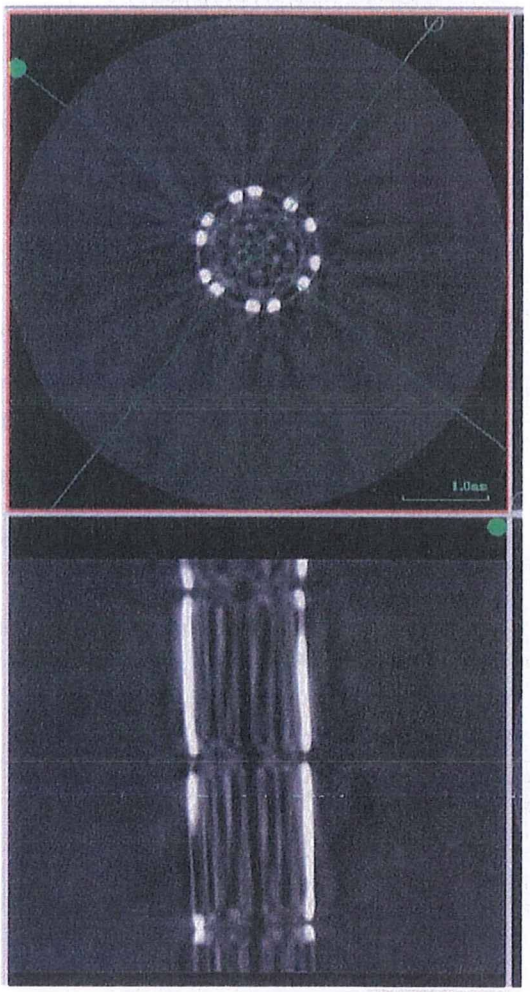

Figure 3. *3-D reconstruction of ICS with gathering all fluoroscopic data. The upper is the PA projection and the lower is the LA view.*

The reconstructed stent is composed of 170,948 triangles and 85,478 points in $3.39 \times 3.34 \times 4.76\,mm^3$ without any bad edges or bad contours. Compared to an ideal stent based on CAD showing an example in Figure 6 with one triangle layer covering on the surface, the surface geometry of micro-CT based is much smoother and more complex.

Figure 7 shows the 3-D reconstruction of a patient geometry with a stent strut based on STL format in the LA view and the PA view is shown in Figure 8. The stent strut of micro-CT is more irregular and is of disordered expansion when compared to a CAD stent.

DISCUSSION

The possibility of decreasing the speed of blood flow in a cerebral aneurysm after stenting has been investigated by experiments with *in vitro* model and computational fluid simulations. Barath et al. (2004, 2005) integrated 20 stents into an *in vitro* circular system and investigated the effect of the stents on the blood flow speed in an aneurysm.

The computational simulation has been widely used for the finding mechanisms, such as blood flow patterns in aneurysms, the wall shear stress (WSS), and the oscillatory shear stress (Cebral and Lohner, 2005; Castro et al., 2006). Most papers have used simplified stent geometries (Stuhne and Steinman, 2004) because of the difficulties of measuring the geometry. The integration of stent geometry to the computational simulation may exhibit the role of stent on blood flow in/on each aneurysm.

Micro-CT can be one of the feasible tools to detect the geometry of an implant, such as a stent with micron scale. The spatial resolution of micro-CT in this study is around 10 μm/pixel and so the struts are enough to be detected.

The reflection of X-ray may decrease the image quality and the boundary condition of the surface of struts. To avoid the effect of reflection on the surface reconstruction, the micro-CT has an integrating system and the threshold can be clear to separate the boundary.

The micro-CT may be also a feasible tool to observe the comparison of recoil with computational simulations. As the balloon expansion may not be isotropic and the residual stress is in the material, recoil may occur (Schmidt et al., 2002). By comparing with the geometry based on CAD, the irregular disposition of strut after the expansion can be detected. Moreover, the recoil or fracture of the stent will be simulated in detail when the micro-CT detects a defect in the stent strut.

The 3-D reconstruction of the stent with STL format has a potential to input the stent geometry data to computational flow simulation of blood flow in an aneurysm when integrating the geometry of the stent

into a patient's data. These techniques will develop a pre-operative simulation allowing selection of the best stent to each patient and also help to solve the diverter function of the stent. Moreover, the design of the stent strut may be considerable to decrease flow speed in an aneurysm.

However, the current technologies of the micro-CT are still not enough to detect dynamic movements such as expansion of a stent because the detection time is still around 20 s for 360°. Therefore, the dynamic movements are necessary to slow rather than the natural state. He et al. (2006) applied micro-CT to blood flow in rat by changing the injection time.

The number of triangles of STL format in this study is over 15,000 and it may be too large. Since the current

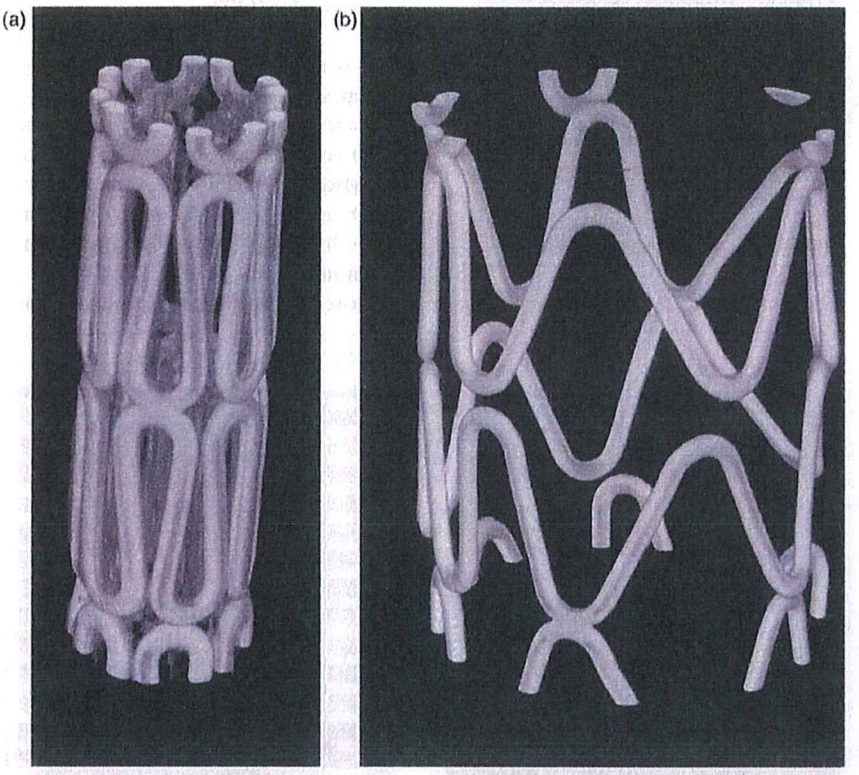

Figure 4. 3-D reconstruction of the stent after selecting a proper threshold: (a) before expansion and (b) after expansion.

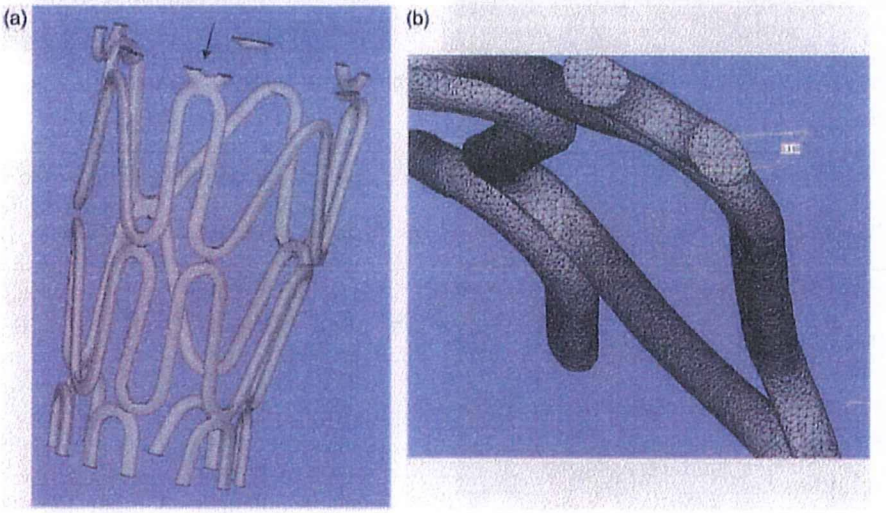

Figure 5. The 3-D reconstruction of the expanded stent after converting to STL format: (a) stent body and (b) stent edge with mesh from the view of arrow in (a).

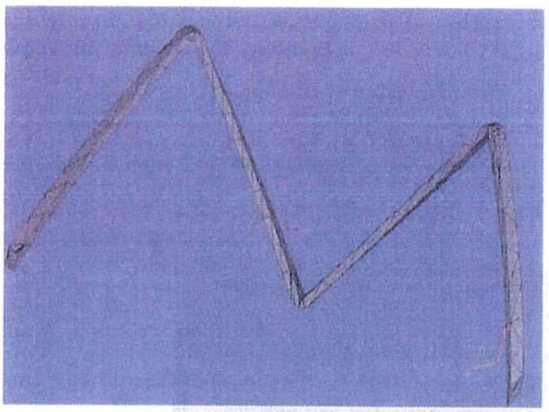

Figure 6. *An example of an expanded stent based on CAD. Only one triangle layer covers one surface. The curved surface has complex triangles.*

normal computational simulations of cerebral aneurysms is 50,000–2,000,000 including spatial and surface meshes, the number of triangles of a stent may be necessary to decrease. Otherwise more powerful computational simulations tools of software and hardware will be necessary in the near future.

CONCLUSIONS

Three-dimensional reconstruction of a cerebral aneurysm with STL format is performed and the geometry is integrated into a cerebral aneurysm from 3-D reconstruction from rotational angiography.

Micro-CT has a possibility of detecting the 3-D geometry of a small implant, such as ICS and may be useful for 3-D reconstruction and integration to computational simulation. And the simulation has a potential to be pre-operative simulation.

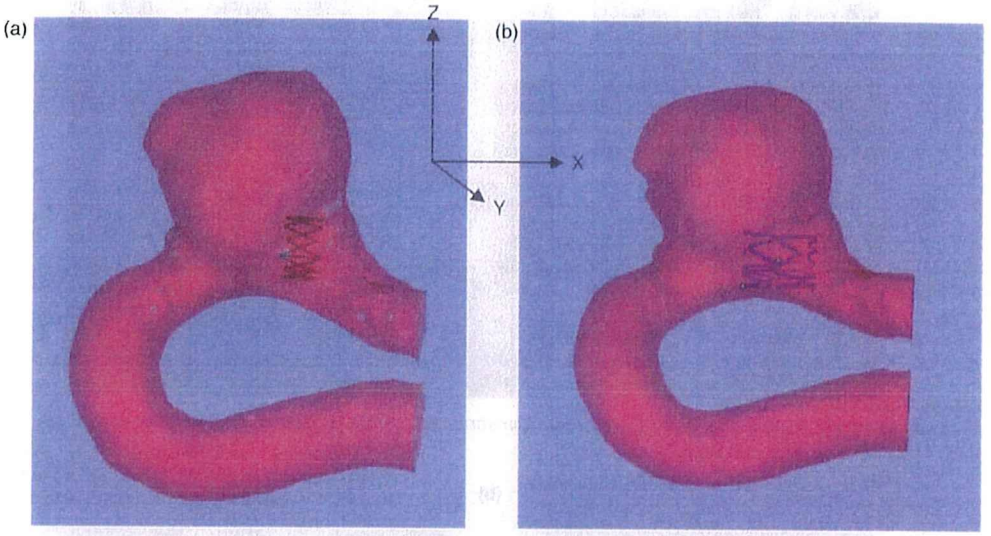

Figure 7. *A patient geometry with a stent strut based on: (a) CAD and (b) micro-CT in the X–Z plane view.*

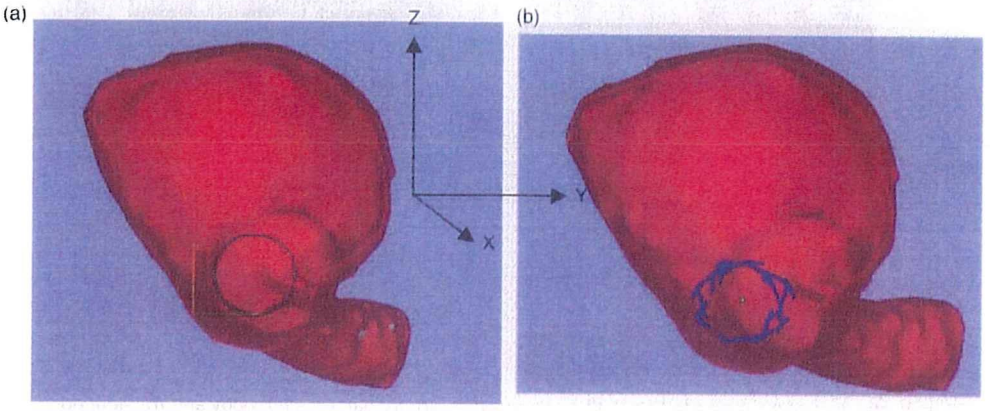

Figure 8. *The PA views on the 3-D reconstruction of patient with a stent based on: (a) CAD and (b) micro-CT.*

ACKNOWLEDGMENTS

The authors are thankful to COOK-WCE, Medtronic, and Shimadzu corporations for helping this study.

REFERENCES

Aenis, M., Stancampiano, A.P., Wakhloo, A.K. and Lieber, B.B. 1997. "Modeling of Flow in a Straight Stented and Nonstented Side Wall Aneurysm Model," *J. Biomech. Eng.*, 119:206–212.

Barath, K., Cassot, F., Rufenacht, D.A. and Fasel, J.H. 2004. "Anatomically Shaped Internal Carotid Artery Aneurysm in Vitro Model for Flow Analysis to Evaluate Stent Effect," *AJNR Am. J. Neuroradiol.*, 25:1750–1759.

Barath, K., Cassot, F., Fasel, J.H., Ohta, M. and Rufenacht, D.A. 2005. "Influence of Stent Properties on the Alteration of Cerebral Intra-Aneurysmal Haemodynamics: Flow Quantification in Elastic Sidewall Aneurysm Models," *Neurol. Res.*, 27(1): S120–128.

Castro, M.A., Putman, C.M. and Cebral, J.R. 2006. "Computational Fluid Dynamics Modeling of Intracranial Aneurysms: Effects of Parent Artery Segmentation on Intra-Aneurysmal Hemodynamics," *AJNR Am. J. Neuroradiol.*, 27:1703–1709.

Cebral, J.R. and Lohner, R. 2005. "Efficient Simulation of Blood Flow Past Complex Endovascular Devices Using an Adaptive Embedding Technique," *IEEE Trans. Med. Imaging*, 24:468–476.

Cebral, J.R., Castro, M.A., Appanaboyina, S., Putman, C.M., Millan, D. and Frangi, A.F. 2005. "Efficient Pipeline for Image-Based Patient-Specific Analysis of Cerebral Aneurysm Hemodynamics: Technique and Sensitivity," *IEEE Trans. Med. Imaging*, 24:457–467.

Cheema, A.N., Hong, T., Nili, N., Segev, A., Moffat, J.G., Lipson, K.E., Howlett, A.R., Holdsworth, D.W., Cole, M.J., Qiang, B., Kolodgie, F., Virmani, R., Stewart, D.J. and Strauss, B.H. 2006. "Adventitial Microvessel Formation after Coronary Stenting and the Effects of Su11218, a Tyrosine Kinase Inhibitor," *J. Am. Coll. Cardiol.*, 47:1067–1075.

D'Urso, P.S., Thompson, R.G., Atkinson, R.L., Weidmann, M. J., Redmond, M.J., Hall, B.I., Jeavons, S.J., Benson, M.D. and Earwaker, W.J. 1999. "Cerebrovascular Biomodelling: A Technical Note," *Surg. Neurol.*, 52:490–500.

Fiorella, D., Albuquerque, F.C., Han, P. and McDougall, C.G. 2004. "Preliminary Experience Using the Neuroform Stent for the Treatment of Cerebral Aneurysms," *Neurosurgery*, 54:6–16; discussion 16–17.

Hassan, T., Timofeev, E.V., Ezura, M., Saito, T., Takahashi, A., Takayama, K. and Yoshimoto, T. 2003. "Hemodynamic Analysis of an Adult Vein of Galen Aneurysm Malformation by Use of 3D Image-Based Computational Fluid Dynamics," *AJNR Am. J. Neuroradiol.*, 24:1075–1082.

He, C., Nakayama, T., Ohta, M. and Takahashi, A. 2006. "Three Dimensions Image of Cerebral Vascular for Computational Fluid Dynamics in Rat: Feasibility of Assessment with Micro-CT," Proceedings of the Third International Symposium on Transdisciplinary Fluid Integration, pp. 59–60.

Hirabayashi, M., Ohta, M., Rufenacht, D.A. and Chopard, B. 2003. "Characterization of Flow Reduction Properties in an Aneurysm Due to a Stent," *Phys. Rev. E Stat. Nonlin. Soft Matter Phys.*, 68:021918.

Jiang, Y., Zhao, J., White, D.L. and Genant, H.K. 2000. "Micro CT and Micro Mr Imaging of 3D Architecture of Animal Skeleton," *J. Musculoskelet. Neuronal Interact.*, 1:45–51.

Langheinrich, A.C., Zoerb, C., Jajima, J., Lommel, D., Walker, G., Mueller, K.M., Rau, W. S. and Bohle, R. 2005. "Quantification of in-Stent Restenosis Parameters in Rabbits by Micro-CT," *Rofo*, 177:501–506.

Molyneux, A., Kerr, R., Stratton, I., Sandercock, P., Clarke, M., Shrimpton, J. and Holman, R. 2002. "International Subarachnoid Aneurysm Trial (ISAT) of Neurosurgical Clipping Versus Endovascular Coiling in 2143 Patients with Ruptured Intracranial Aneurysms: A Randomised Trial," *Lancet*, 360:1267–1274.

Ohta, M., Handa, A., Iwata, H., Rufenacht, D.A. and Tsutsumi, S. 2004a. "Poly-Vinyl Alcohol Hydrogel Vascular Models for in Vitro Aneurysm Simulations: The Key to Low Friction Surfaces," *Technol. Health Care*, 12:225–233.

Ohta, M., Hirabayashi, M., Wetzel, S., Lylyk, P., Iwata, H., Tsutsumi, S. and Rufenacht, D.A. 2004b. "Impact of Stent Design on Intra-Aneurysmal Flow: A Computer Simulation Study," *Interventional Neuroradiology*, 10:85–94.

Schmidt, W., Andresen, R., Behrens, P. and Schmitz, K.P. 2002. "Characteristic Mechanical Properties of Balloon-Expandable Peripheral Stent Systems," *Rofo Fortschr Geb Rontgenstr Neuen Bildgeb Verfahr*, 174:1430–1437.

Shojima, M., Oshima, M., Takagi, K., Torii, R., Nagata, K., Shirouzu, I., Morita, A. and Kirino, T. 2005. "Role of the Bloodstream Impacting Force and the Local Pressure Elevation in the Rupture of Cerebral Aneurysms," *Stroke*, 36:1933–1938.

Steinman, D.A., Milner, J.S., Norley, C.J., Lownie, S.P. and Holdsworth, D.W. 2003. "Image-Based Computational Simulation of Flow Dynamics in a Giant Intracranial Aneurysm," *AJNR Am. J. Neuroradiol.*, 24:559–566.

Stuhne, G.R. and Steinman, D.A. 2004. "Finite-Element Modeling of the Hemodynamics of Stented Aneurysms," *J. Biomech. Eng.*, 126:382–387.

Wetzel, S.G., Ohta, M., Handa, A., Auer, J.M., Lylyk, P., Lovblad, K.O., Babic, D. and Rufenacht, D.A. 2005. "From Patient to Model: Stereolithographic Modeling of the Cerebral Vasculature Based on Rotational Angiography," *AJNR Am. J. Neuroradiol.*, 26:1425–1427.

Yoshida, H., Kakino, T., Kajitani, M., Goh, K., Gohda, T., Yasuda, K. and Tanabe, T. 1991. "Transcatheter Placement of an Intraluminal Prosthesis for the Thoracic Aorta. A New Approach to Aortic Dissections," *ASAIO Trans.*, 37:M272–273.

Takashi Kandori
Graduate School of Engineering,
Tohoku University,
6-6 Aramaki-Aoba,
Aoba-ku, Sendai 980-8579, Japan

Toshiyuki Hayase[1]
Institute of Fluid Science,
Tohoku University,
2-1-1 Katahira,
Aoba-ku, Sendai 980-8577 Japan

Kousuke Inoue

Kenichi Funamoto

Takanori Takeno

Institute for International Advanced
Interdisciplinary Research,
International Advanced Research and
Education Organization,
Tohoku University,
6-3 Aramaki-Aoba,
Aoba-ku, Sendai 980-8578, Japan

Makoto Ohta
Institute of Fluid Science,
Tohoku University,
2-1-1 Katahira,
Aoba-ku, Sendai 980-8577 Japan

Motohiro Takeda
Graduate School of Medicine,
Tohoku University,
2-1 Seiryo-machi,
Aoba-ku, Sendai 980-8574, Japan

Atsushi Shirai
Institute of Fluid Science
Tohoku University,
2-1-1 Katahira,
Aoba-ku, Sendai 980-8577 Japan

Frictional Characteristics of Erythrocytes on Coated Glass Plates Subject to Inclined Centrifugal Forces

In recent years a diamond-like carbon (DLC) film and a 2-methacryloyloxyethyl phosphorylcholine (MPC) polymer have attracted attention as coating materials for implantable artificial organs or devices. When these materials are coated on vascular devices, compatibility to blood is an important problem. The present paper focuses on friction characteristics of erythrocytes to these coating materials in a medium. With an inclined centrifuge microscope developed by the authors, observation was made for erythrocytes moving on flat glass plates with and without coating in a medium of plasma or saline under the effect of inclined centrifugal force. Friction characteristics of erythrocytes with respect to these coating materials were then measured and compared to each other to characterize DLC and MPC as coating materials. The friction characteristics of erythrocytes in plasma using the DLC-coated and noncoated glass plates are similar, changing approximately proportional to the 0.5th power of the cell velocity. The cells stick to these plates in saline as well, implying the influence of plasma protein. The results using the MPC-coated plate in plasma are similar to those of the other plates for large cell velocities, but deviate from the other results with decreased cell velocity. The results change nearly proportional to the 0.75th power of the cell velocity in the range of small velocities. The results for the MPC-coated plate in saline are similar to that in plasma but somewhat smaller, implying that the friction characteristics for the MPC-coated plate are essentially independent of plasma protein. [DOI: 10.1115/1.2948420]

Keywords: erythrocytes, friction characteristics, inclined centrifuge microscope, DLC, MPC polymer, glass plate, plasma

1 Introduction

Blood flow in microcirculation plays an important role in supplying tissues with nutrients and removing metastases. Extensive physiological research has been carried out to examine blood flow in microcirculation focusing on the complex interaction between blood cells, plasma proteins, and glycocalyx in the endothelial surface layer [1,2]. Numerical analysis has been performed for cell motion in a blood capillary considering the interaction between the cell and the endothelial surface layer [3], but there have been little experimental measurement data of friction characteristics to date. It is critically important to develop a method to measure this friction force acting on the blood cells moving along the vessel surface.

The centrifuge microscope enables us to observe cells under centrifugal force [4], and, to date, several different types of centrifuge microscope have been developed [5]. These devices have been used to investigate various cell characteristics, for example, the mechanical properties of the Echinoderm egg [6], the motive force of paramecia [7], and the force-velocity relation of muscle fibers [8]. However, all existing centrifuge microscopes are designed such that the direction of cell deformation or movement and the direction of centrifugal force are identical, and the magnitude of the centrifugal force is the only parameter to be specified (see Fig. 1(*a*)). The present study uses the inclined centrifuge microscope [9], which enables us to observe cells on an inclined plane while specifying the tangential and normal force components of the centrifugal force independently (Fig. 1(*b*)). In order to gain a fundamental understanding of the blood cell interaction

[1]Corresponding author.

Contributed by the Bioengineering Division of ASME for publication in the JOURNAL OF BIOMECHANICAL ENGINEERING. Manuscript received August 23, 2007; final manuscript received March 11, 2008; published online July 14, 2008. Review conducted by Fumihiko Kajiya.

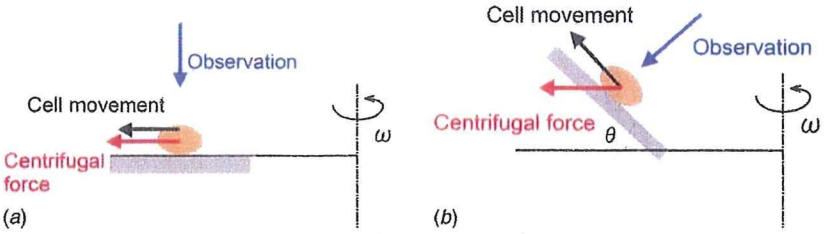

Fig. 1 Comparison between conventional and inclined centrifuge microscope: (*a*) conventional centrifuge microscope and (*b*) inclined centrifuge microscope

mentioned above, the present study investigated the friction characteristics of erythrocytes moving along material-coated glass plates in plasma or saline using the inclined centrifuge microscope.

In recent years materials for coating implantable artificial organs or devices have attracted attention. Among them this paper deals with diamond-like carbon (DLC) film [10] and 2-methacryloyloxyethyl phosphorylcholine (MPC) polymer [11]. DLC is one of the carbon based coatings with amorphous structure, which has properties similar to diamond. It has good resistance to corrosion and wear, low coefficient of friction, low partner aggressiveness, superflat smoothness, a thin film, and insulation properties. MPC was developed to create biomembrane structures artificially. It has a phosphorylcholine base that has a phospholipid polar group side chain and has a characteristic to restrain proteinaceous absorption.

When the DLC or MPC polymer is coated on vascular devices, compatibility to blood is an important problem. The present paper focuses on friction characteristics of erythrocytes to these coating materials in a medium. The inclined centrifuge microscope is used first to observe the motion of erythrocytes moving on flat glass plates with and without coating of DLC or MPC polymer in a medium of plasma or saline under the effect of centrifugal force at an angle with respect to the plate. Friction characteristics of erythrocytes to these materials are then measured and compared with each other to characterize DLC and MPC polymer as a coating material from the viewpoint of the friction property of erythrocytes.

2 Experimental Apparatus and Principle

2.1 Inclined Centrifuge Microscope. A schematic and specifications of the inclined centrifuge microscope system are shown in Fig. 2 and Table 1, respectively. In order to improve measurement performance, several components of the original equipment [9] have been replaced in the present system. A pair of inclined containers of inner dimension of $10 \times 8 \times 1$ mm^3 (width × length × height) is mounted on the rotor of the centrifuge (KUBOTA, Model 1120). One of the two containers is filled with a medium containing blood cells and the other container remains empty. The rotation speed of the rotor is measured using a digital tachometer (ONO SOKKI, TM-2110, error: 0.02%). A reference signal of rotation, which is generated by a laser diode (NEO ARK, LDP-6930C) and a detector (NEO ARK, RD-102), and is delayed through a pulse generator (Hewlett-Packard, HP81101A, 50 MHz) and a signal synthesizer (NF Circuit Design Block, WF1944), triggers an yttrium aluminum garnet (YAG) laser (KANOMAX, SPIV-30-20-ATT, 3 ns/pulse, 30 mJ/pulse) and a charge coupled device (CCD) camera (Ikegami, SKC-141, 15 fps, 145 megapixels). The exposure time of the CCD camera is fixed at 1/8000 s and the exposure timing is controlled to accurately synchronize with the rotation. The laser beam, which is guided through an optical fiber (NIKON, GFLG-5), illuminates the container for a very short interval of 3 ns during the exposure time of the CCD camera at the same angular position of the spinning rotor so that a still image of the plate can be observed. Erythrocytes moving on the plate are observed through a microscope (NIKON, CM-10) with objectives (Olympus, Cplan F1 10× and CF Plan EPI SLWD 50×), the light axis of which is adjusted normal to the plate at an angle of θ from the horizontal plane. The microscope was remodeled to change the optical axis 90 deg by mirroring at the connecting point of the objective lens. The images are sent to a PC and stored on its hard drive.

In each measurement, 100 sequential images with an interval of the smallest multiple of the rotation period larger than 1/15 s were obtained. Each image was digitized into 1392 × 1024 pixels with a 256-level monochrome gradation and a diameter of 0.65 μm/pixel for the 10× objective lens. Fluctuation of the images due to inevitable error in synchronization was removed by translating the images based on grid lines of 5 μm in width etched on the back of the plates. The image data were

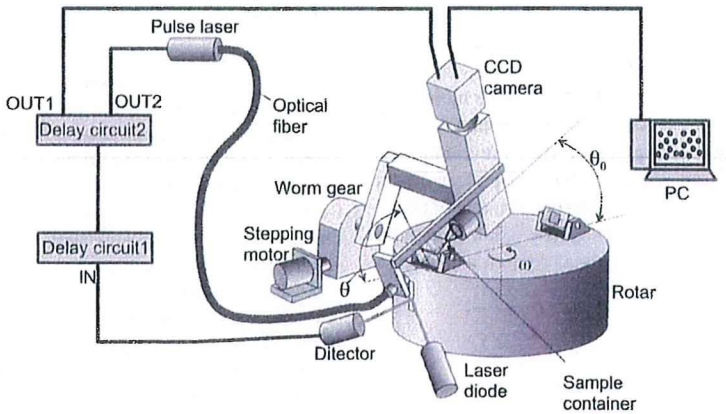

Fig. 2 Schematic of the inclined centrifuge microscope system